

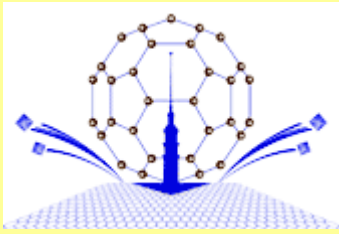
"Advanced Carbon Nanostructures" (ACN'2011)
St.Petersburg, Russia, July 4-8, 2011



Raman characterization of nanostructured graphite materials

Baranov A.V.

*St.Petersburg State University of Information Technologies,
Mechanics and Optics, 19710, St.Petersburg, Russia
e-mail: a_v_baranov@yahoo.com*



"Advanced Carbon Nanostructures" (ACN'2011)
St.Petersburg, Russia, July 4-8, 2011



Raman background (classical)

Energy irradiated by dipole \mathbf{P} with frequency ω per time unit and per solid angle $d\Theta$,

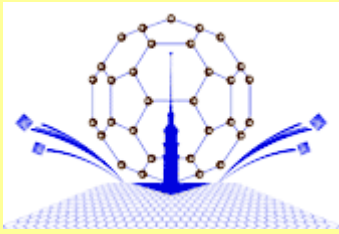
$$\frac{dW}{d\Theta} = \frac{\omega^4}{(4\pi)^2 \varepsilon_0 c^3} |\mathbf{e}_s \mathbf{P}|^2$$

$\mathbf{P} = \alpha \mathbf{E}$, where \mathbf{E} - electric field strength, α – the polarizability (Raman) tensor with components α_{ij} ($i, j - x, y$ и z)

$$\begin{bmatrix} \alpha_{xx} & \alpha_{xy} & \alpha_{xz} \\ \alpha_{yx} & \alpha_{yy} & \alpha_{yz} \\ \alpha_{zx} & \alpha_{zy} & \alpha_{zz} \end{bmatrix}$$

series expansion of α_{ij} for normal vibrations l over coordinate Q_l near equilibrium point

$$\alpha_{ij}(Q_l) = \alpha_{ij}^0 + \left(\frac{\partial \alpha_{ij}}{\partial Q_l} \right)_0 Q_l + \frac{1}{2} \left(\frac{\partial^2 \alpha_{ij}}{\partial Q_l^2} \right)_0 Q_l^2 + \dots$$



Raman background (classical)

$$Q_l = Q_{0l} \times \cos(\omega_v t) \quad E = E_0 \times \cos(\omega_L t)$$

$$\begin{aligned}
 P_i(\omega_v, \omega_L) = & \alpha_{ij}^0 E_{0j} + \alpha_{ij}^0 E_{0j} \cos(\omega_L t) + \frac{1}{2} \left(\frac{\partial \alpha_{ij}}{\partial Q_l} \right)_0 E_{0j} Q_{0l} \cos[(\omega_L - \omega_v)t] + \\
 & + \frac{1}{2} \left(\frac{\partial \alpha_{ij}}{\partial Q_l} \right)_0 E_{0j} Q_{0l} \cos[(\omega_L + \omega_v)t] + \frac{1}{4} \left(\frac{\partial^2 \alpha_{ij}}{\partial Q_l^2} \right)_0 E_{0j} Q_{0l}^2 \cos[(\omega_L - 2\omega_v)t] + \\
 & + \frac{1}{4} \left(\frac{\partial^2 \alpha_{ij}}{\partial Q_l^2} \right)_0 E_{0j} Q_{0l}^2 \cos[(\omega_L + 2\omega_v)t] + \dots
 \end{aligned}$$

where: 2 term – the Rayleigh scattering;

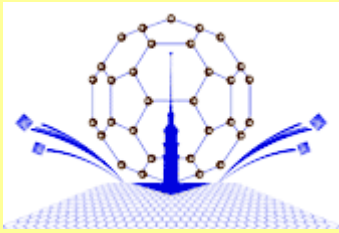
others – Raman scattering.

3 and 4 terms - Stokes and Antistokes Raman with $\omega_s = \omega_L - \omega_v$ and $\omega_s = \omega_L + \omega_v$

5 and 6 terms - second order Stokes and Antistokes Raman with $\omega_s = \omega_L - 2\omega_v$ и $\omega_s = \omega_L + 2\omega_v$

For 2 vibrations (l and m with ω_{v1} and ω_{v2}) the terms like $\frac{1}{2} \left(\frac{\partial^2 \alpha_{ij}}{\partial Q_l \partial Q_m} \right)_0 Q_{0l} Q_{0m}$ with

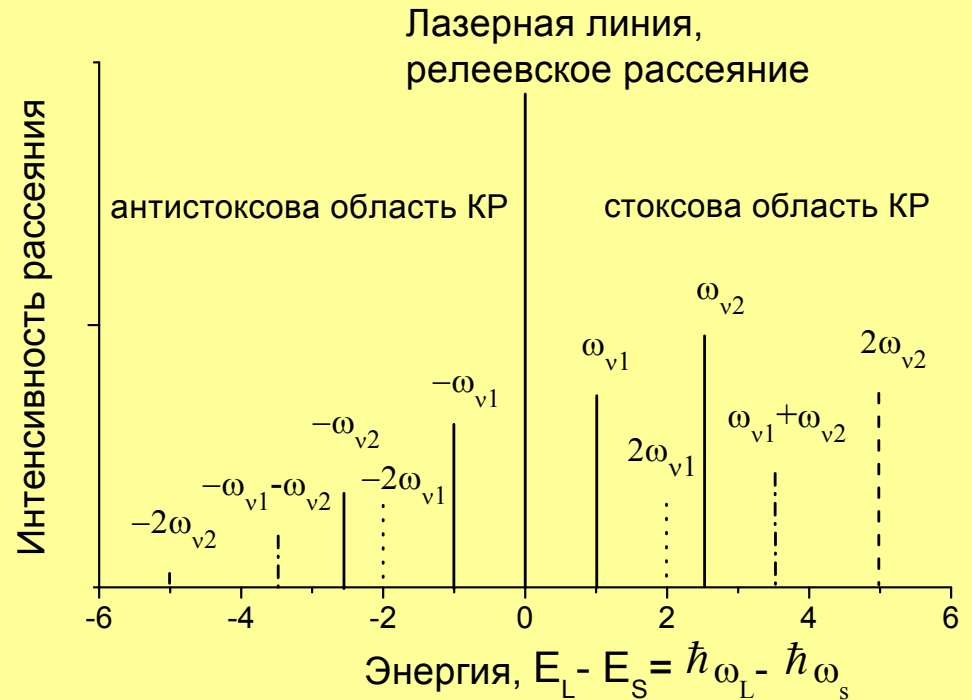
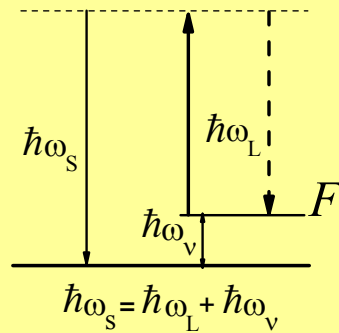
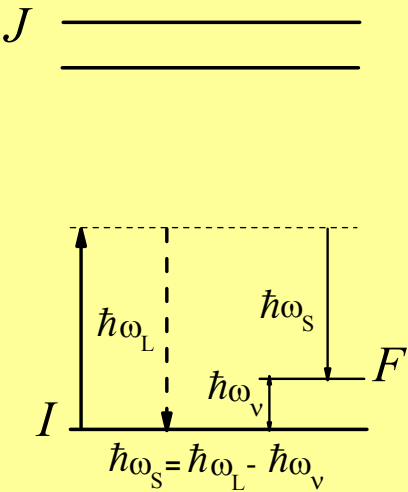
frequencies $(\omega_L + \omega_{v1} - \omega_{v2})$, $(\omega_L - \omega_{v1} + \omega_{v2})$, $(\omega_L + \omega_{v1} + \omega_{v2})$ and $(\omega_L - \omega_{v1} - \omega_{v2})$ will appear.

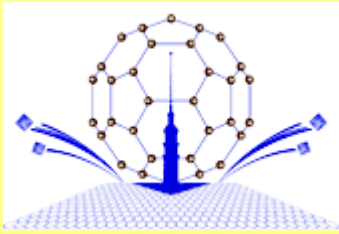


Raman background (classical)

стоксово КР

антистоксово КР





Raman background (classical)

Raman power per unit of solid angle

$$\frac{dW^{KP}}{d\Theta} = \frac{\omega_S^4}{(4\pi)^2 \epsilon_0 c^3} |\mathbf{e}_S \hat{\alpha} \mathbf{e}_L|^2 Q_{0l}^2 E_0^2$$

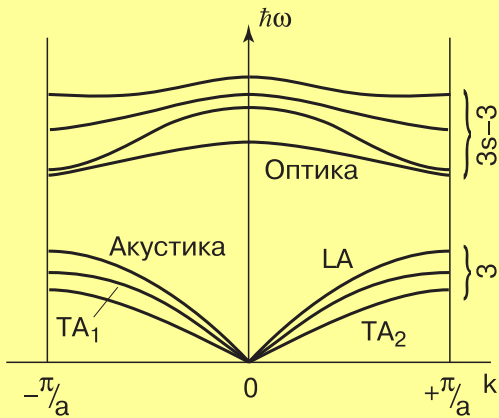
Raman differential cross-section

$$\frac{d\sigma^{KP}}{d\Theta} = \frac{\omega_S^4}{(4\pi\epsilon_0)^2 c^4} |\mathbf{e}_S \hat{\alpha} \mathbf{e}_L|^2 Q_{0l}^2$$

Raman conservation laws:

$$\hbar\omega_L = \hbar\omega_S \pm \hbar\omega_V - \text{energy}$$

$$\mathbf{k}_L = \mathbf{k}_S \pm \mathbf{q} - \text{momentum (wave vector)}$$

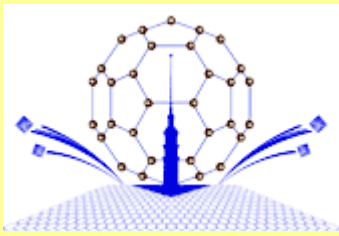


Phonon dispersion curves

$$\mathbf{k}_L \sim \mathbf{k}_S \sim 2 \times 10^6 \text{ m}^{-1}, \quad \pi/a \sim 10^{10} \text{ m}^{-1}$$

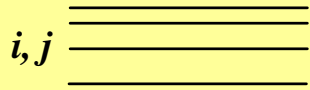
1st order Raman - phonons with small \mathbf{q} (center of Brillouin zone)

2nd order Raman – phonon with any \mathbf{q} (density of phonon states)

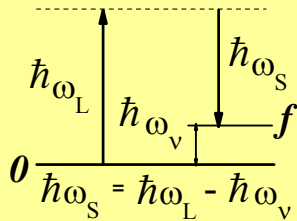


Raman background (quantum-mechanical)

Raman cross-section

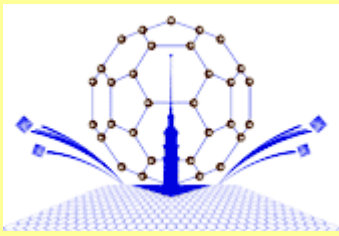


$$\frac{d\sigma^{KP}}{d\Theta}(\mathbf{k}_L\omega_L, \mathbf{k}_S\omega_S) = \frac{\omega_L^2\omega_S^2}{(4\pi\epsilon_0)^2 c^4} |K_{f,0}|^2 \delta(E_f - E_L + E_S)$$



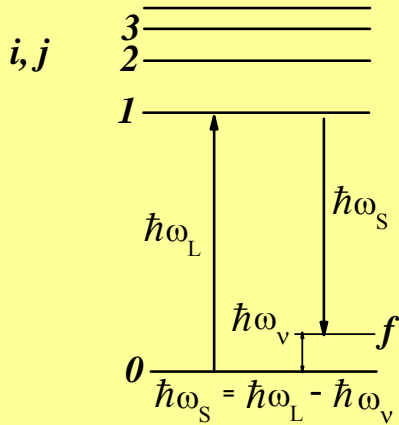
Composite matrix element

$$K_{f,0} = \sum_{ij} \left[\frac{M_{ff} M_{ji} M_{io}}{(\hbar\omega_L - \hbar\omega_i^e - i\hbar\gamma_i)(\hbar\omega_S - \hbar\omega_j^e - i\hbar\gamma_j)} \right]$$



Raman background (quantum-mechanical)

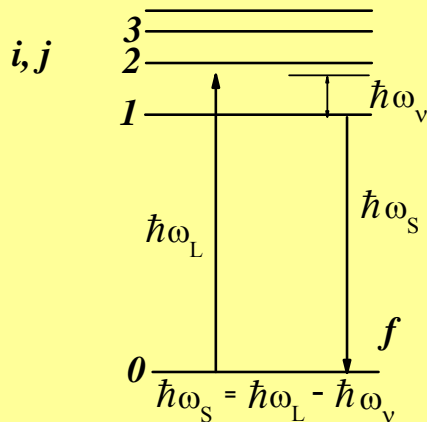
Resonant Raman



$$K_{f,0} = \sum_{ij} \left[\frac{M_{ff} M_{ji} M_{io}}{(\hbar\omega_L - \hbar\omega_i^e - i\hbar\gamma_i)(\hbar\omega_S - \hbar\omega_j^e - i\hbar\gamma_j)} \right]$$

input resonance

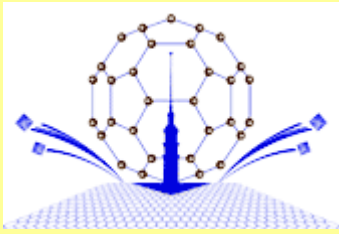
$$\sigma^{KP} \equiv \frac{d\sigma^{KP}}{d\Theta} = const \times \frac{M_{01}^2 \mathbf{M}_{11}^2 M_{01}^2}{(\hbar\omega_L - \hbar\omega_{01} - i\hbar\gamma_{01})^2} \delta(E_f - E_L + E_S)$$



output resonance

$$\sigma^{KP} \equiv \frac{d\sigma^{KP}}{d\Theta} = const \times \frac{M_{01}^2 \mathbf{M}_{11}^2 M_{01}^2}{(\hbar\omega_S - \hbar\omega_{01} - i\hbar\gamma_{01})^2} \delta(E_f - E_L + E_S)$$

Amplification: $n = (\omega_L - \omega_{01})^2 / \gamma^{012}$



"Advanced Carbon Nanostructures" (ACN'2011)
St.Petersburg, Russia, July 4-8, 2011



Raman background (quantum-mechanical)

Resonant Raman. Double coupled resonance (DCR).

$$K_{f,0} = \sum_{ij} \left[\frac{M_{ff} M_{ji} M_{io}}{(\hbar\omega_L - \hbar\omega_i^e - i\hbar\gamma_i)(\hbar\omega_S - \hbar\omega_j^e - i\hbar\gamma_j)} \right]$$

Should be fulfilled
simultaneously

$$\begin{aligned} (\hbar\omega_S - \hbar\omega_j^e - i\hbar\gamma_j) &= 0 \\ (\hbar\omega_L - \hbar\omega_i^e - i\hbar\gamma_i) &= 0 \end{aligned}$$

2-nd order Raman

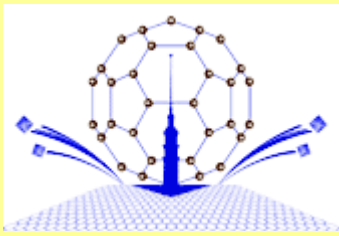
It is possible at large
 $q_{Res} \approx k \gg 0$

materials where momentum conservation
low is violated by nanoscale disorder or
size (nanocrystals) GRAPHYTE

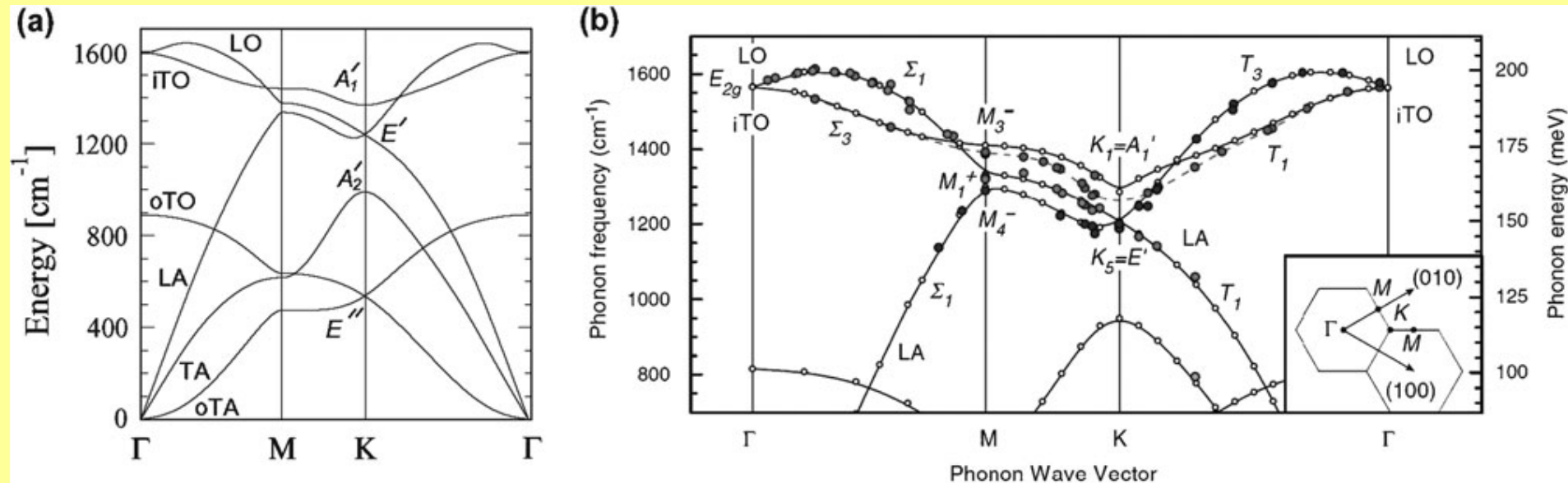
Since $k=k(\omega_L)$ and $\omega_v = \omega_v(q)$, peaks with Stokes shifts depending on incident laser wavelength are observed in the 1-st order Raman spectra

Baranov, A.V. et al., Opt.Spectrosc.1987,62,612; Thomsen, C. et al., PRL, 2000, 85, 5214.

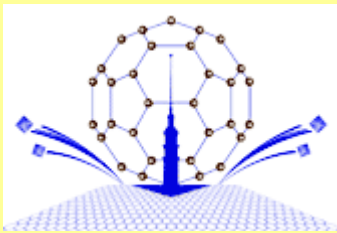
Second International School/Conference for Young Scientists, "Diagnostics of carbon nanostructures"



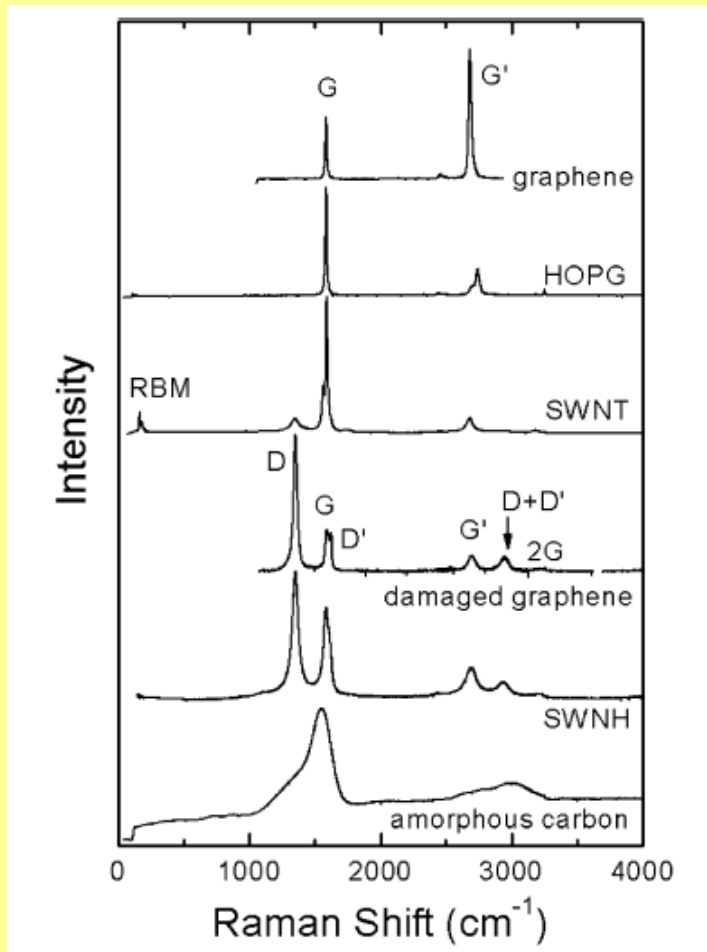
Raman scattering in graphitic materials



(a) Calculated phonon dispersion relations of two dimensional graphite. LO, iTO, oTO, LA, TA and oTA are phonon modes at the Γ point and A_{01} , E_0 , A_{02} , and E_{00} are irreducible representations for phonon modes at the K point. (b) Inelastic X-ray measurements of phonon dispersion relations of graphite.



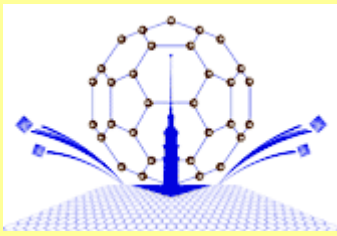
Raman scattering in graphitic materials



Raman spectra from different types of sp² nanocarbons.

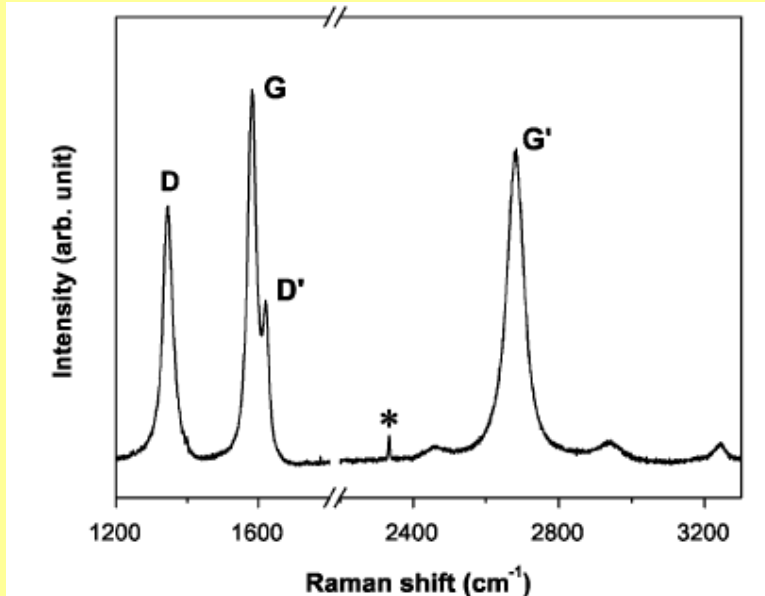
The graphene-related structures are labeled next to their respective spectra. The main features (disorder-induced D, D' and D + D' bands; first-order Raman-allowed G band; and second-order Raman overtones G' (2iTO) and 2G) are labeled in some spectra, but the assignment applies to all of them.

The detailed analysis of the frequency, line shape, and intensity for these features gives a great deal of information about each respective sp² carbon structure. *M.S. Dresselhaus et al., Nano Lett., 2010, 10*



Raman scattering in graphitic materials

The G-band and the disorder-induced D and D' bands, and G', or 2D band

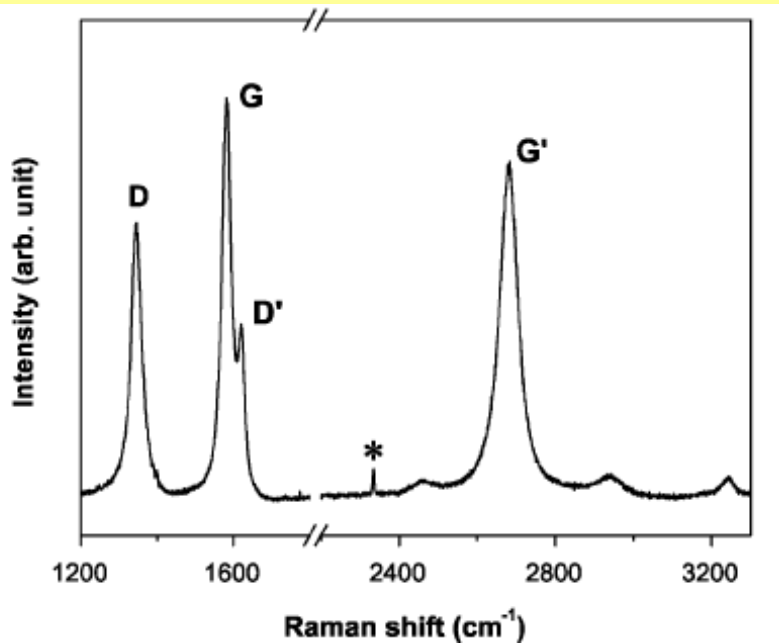


G band at 1582 cm^{-1} (graphite), the D band at about 1350 cm^{-1} , the D'-band at about 1620 cm^{-1} and the G'(2D)-band at about 2700 cm^{-1} (laser excitation wavelength at 514.5 nm). The G band is a doubly degenerate (iTO and LO) phonon mode (E_{2g} symmetry) at the BZ center. Presence the G-band in the Raman spectra means that the sample contains sp^2 carbon networks. In contrast, sp^3 and sp carbon networks show characteristic Raman features at 1333 cm^{-1} (diamond) and in the

range $1850\text{--}2100\text{ cm}^{-1}$ (linear carbon chains), respectively. The D and D' bands are defect induced and these bands cannot be seen for a highly crystalline graphite. The integrated intensity ratio I_D/I_G for the D band and G band is widely used for characterizing the defect quantity in graphitic materials.

Raman scattering in graphitic materials

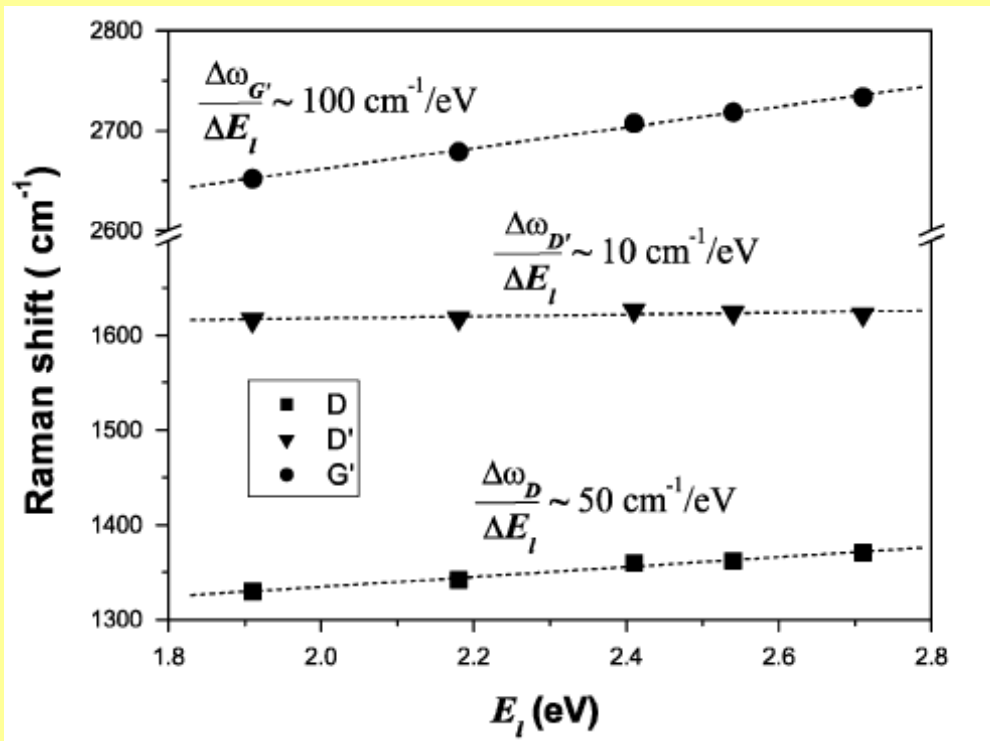
The second-order spectra, G'-band



All kinds of graphitic materials show a strong Raman band which appears in the range 2500–2800 cm^{-1} which corresponds to the overtone of the D band. This band called also the G'-band is observed in the second-order Raman spectra of crystalline graphite without any kind of disorder. The Raman feature at about 2950 cm^{-1} is associated with a D+G combination mode and also is induced by disorder. A common feature of the G'-band and D+G band is dependence of their Stokes shift on the laser excitation wavelength

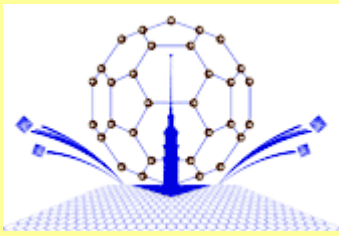
Raman scattering in graphitic materials

Dispersive behavior of the D-band and G'-band. Double resonance evidence.



The slope associated with the G'-band is about 100 cm¹/eV and is two times the slope of the D-band (50 cm¹/eV). The D' band also exhibits a weak dispersive behavior, the slope being about 10 cm¹/eV. The slopes are determined by slopes of both electron and phonon dispersion curves of the materials near K-point of the BZ.

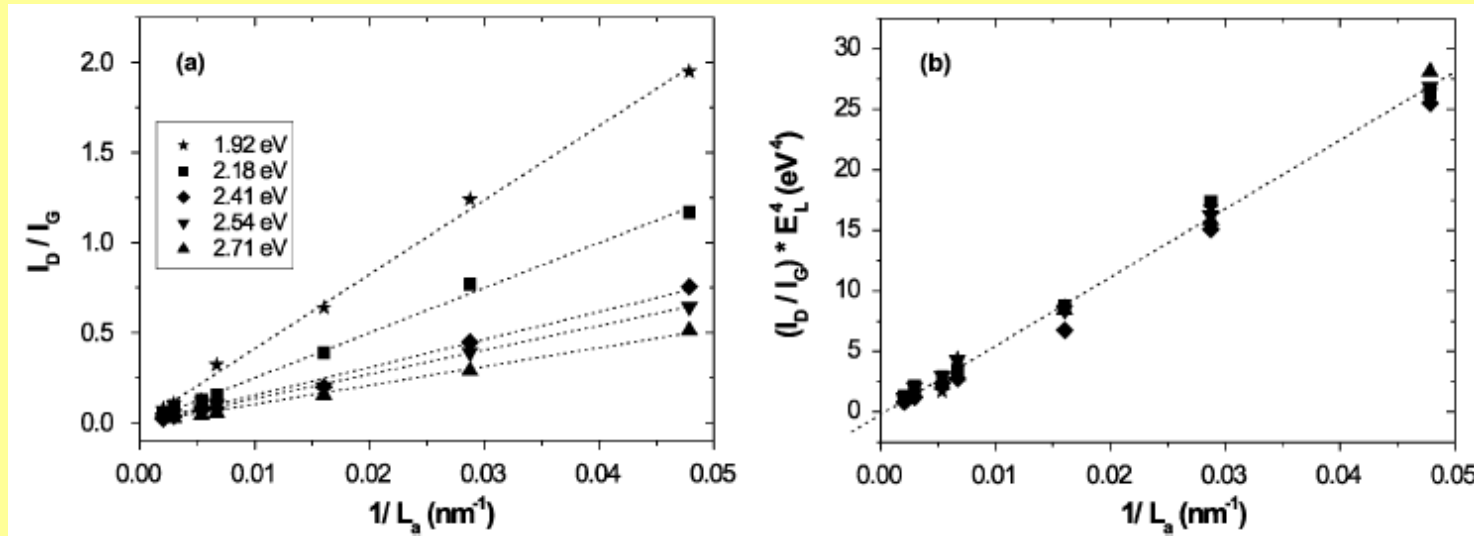
Laser energy dependence of the frequency of the D, D', and G' bands [R. P. Vidano et al., Solid State Commun., 1981, **39**, 341]



Raman scattering in graphitic materials

Crystallite size dependence of the D-band

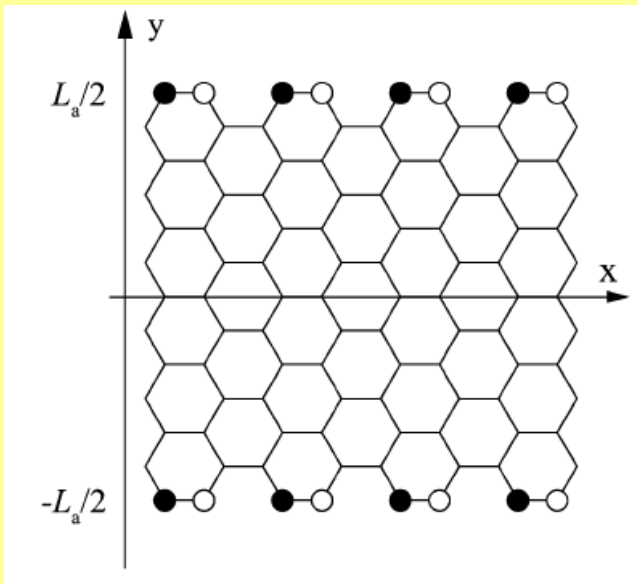
The ratio of the D and G band intensities (I_D/I_G) can be used for estimation of the in-plane crystallite sizes L_a by using the empirical formula $L_a(\text{nm}) = \frac{560}{E_{\text{laser}}^4} \left(\frac{I_D}{I_G} \right)^{-1}$ where E_{laser} is the excitation laser energy in eV used in the Raman experiment.



(a) The intensity ratio I_D/I_G versus $1/L_a$ using five different laser excitation energies is plotted. (b) All curves shown in part (a) collapse on the same curve in the $(I_D/I_G)E_L^4$ versus $1/L_a$ plot where $E_L = E_{\text{laser}}$

Raman scattering in graphitic materials

Edge states.



The model of a nanographite ribbon with the armchair edge at $y = \pm L_a/2$ and zigzag edge along y axis. In the armchair edge, we have two carbon atoms (solid and open circles) which belong to different sublattices A and B of graphite. Because of the lack of symmetry between the A and B sublattices, localized electronic states appear around the zigzag edge, while no edge states appear for armchair edges [K. Nakada, et al. PRB 1996, **54**, 17954.

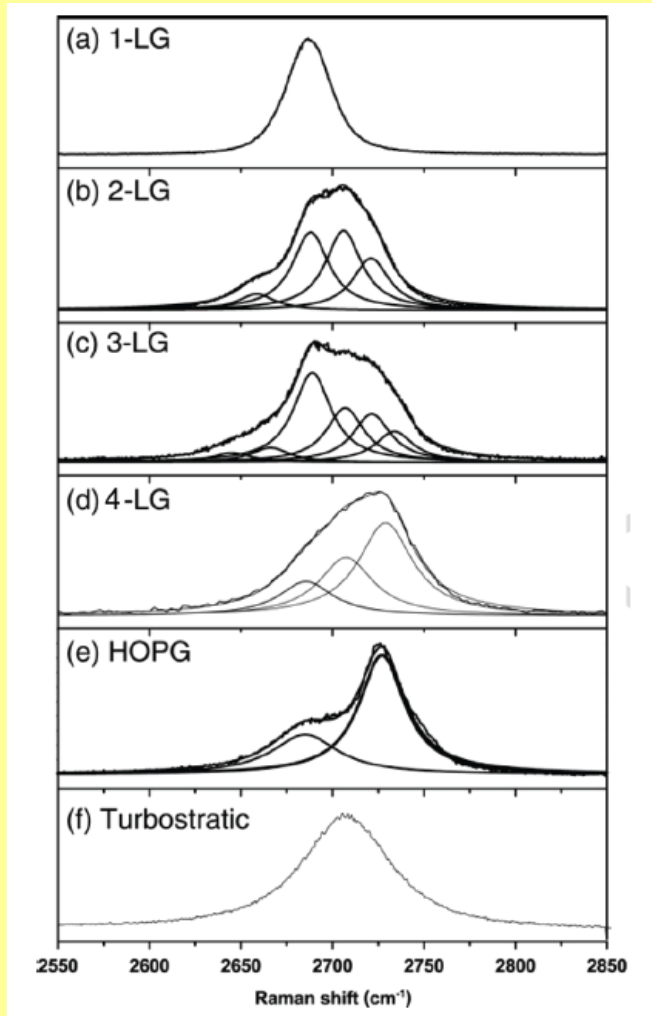
The bands at $\sim 1120 \text{ cm}^{-1}$ (TPA-like) in Raman spectra of nanographites can be associated with vibration localized in the zigzag edges

Raman scattering in graphitic materials

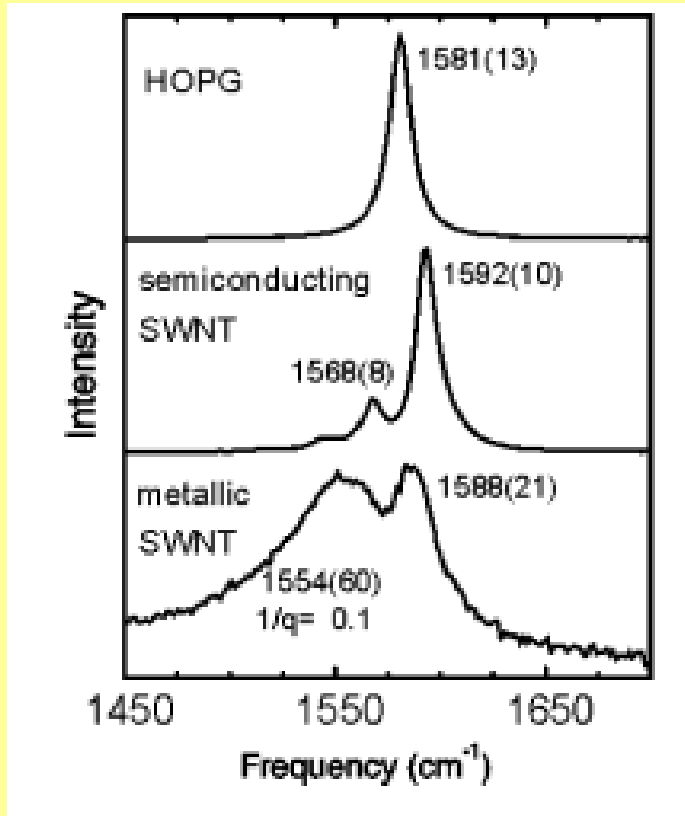
Out-of-plane stacking order

Stacking faults. The hexagonal network of graphite layers is stacked. In turbostratic graphite (nanographite) there is no stacking order between adjacent layers. Because of interlayer interaction for a finite number of graphene planes, we have several 2D (G') energy bands split by discrete k vectors in the c - direction.

← The G' spectra for graphene as a function of the number of layers. [Malard, L. M. et al., *Phys. Rep.* 2009, **473**, 51.]



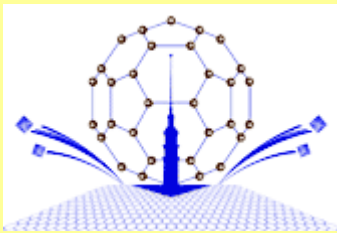
Raman scattering in graphitic materials



The G-band for highly oriented pyrolytic graphite (HOPG), one semiconducting SWNT, and one metallic SWNT

Nanotubes

Curvature effects, such as occur in carbon nanotubes, give rise to multiple peaks in the G-band spectrum for a SWNT, while a single peak ($\omega_G \approx 1582 \text{ cm}^{-1}$) is observed for a 2D graphene sheet. Up to six G-band phonons are Raman allowed in chiral SWNTs, although two of them (the totally symmetric A_1 modes) usually dominate the spectra. This curvature dependence generates a diameter dependence, thus making the G band a probe also for the tube diameter, while the G-band dependence on externally induced strain is very rich and is still controversial. [M.S. Dresselhaus et al., Nano Lett., 2010, 10]

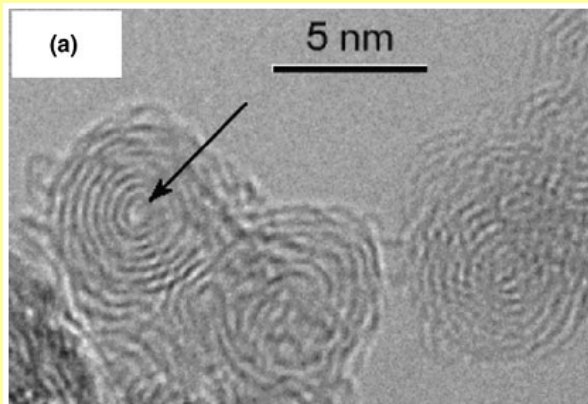


"Advanced Carbon Nanostructures" (ACN'2011)
St.Petersburg, Russia, July 4-8, 2011

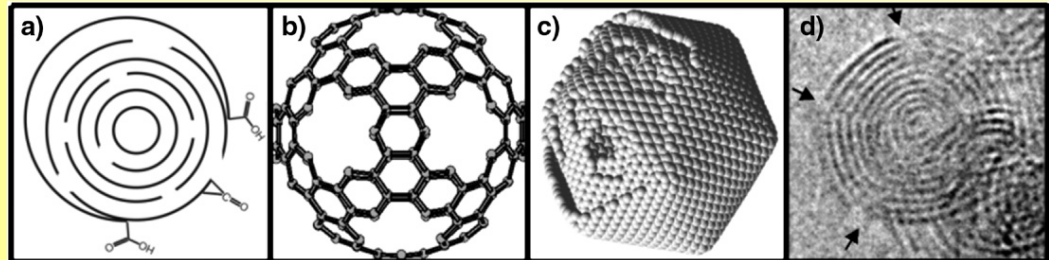


Presence of defects and amorphous phase.

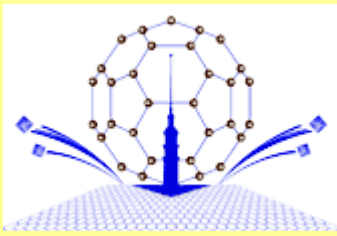
Multishell nanographites (onion-like carbons, OLC) produced by annealing of detonation nanodiamonds



TEM image



Schematic representation of the structure with different types of disorder



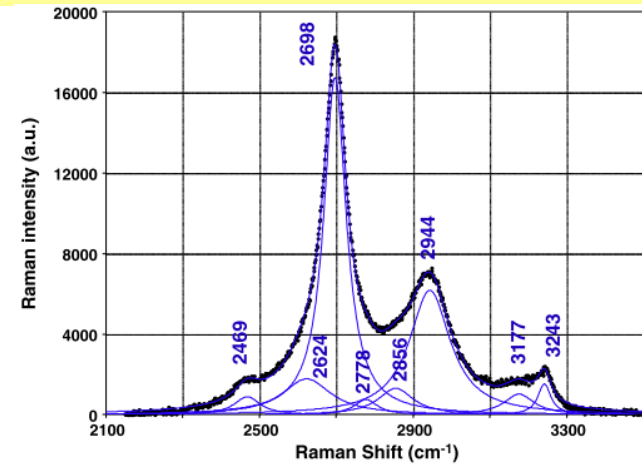
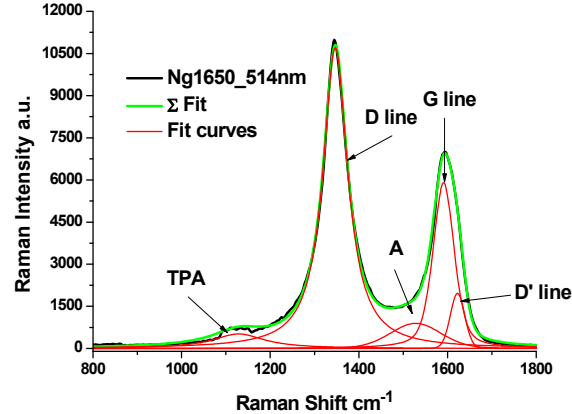
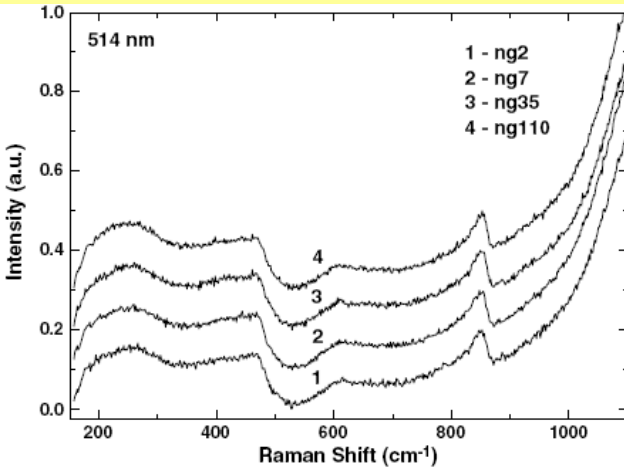
"Advanced Carbon Nanostructures" (ACN'2011)
St.Petersburg, Russia, July 4-8, 2011



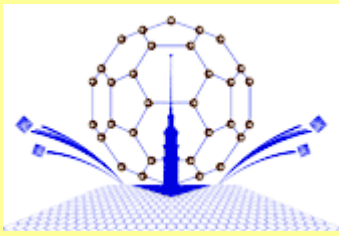
Presence of defects and amorphous phase.

Multishell nanographites (onion-like carbons, OLC) produced by annealing of detonation nanodiamonds

Structural ordering with annealing: $T \sim 1500 - 1650 \text{ }^\circ\text{C}$, time $\sim 2 - 110 \text{ min}$



<1000 cm^{-1} : Phonon density of state. Line 860 cm^{-1} – oTO- phonons (Γ -point).
 1000-1800 cm^{-1} : TPA-line, D- and D'- double resonance lines, A – amorphous carbon line, G - line is the doubly degenerated (iTO and LO) phonon mode (E_{2g}).
 2000-3600 cm^{-1} : 2nd order Raman spectrum – sum and overtones of modes observed in 1st order Raman spectrum.

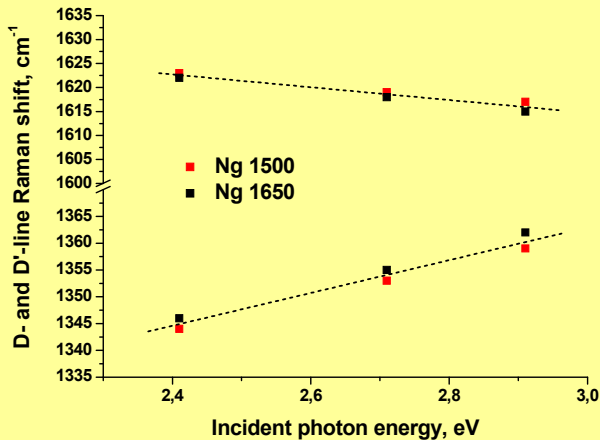
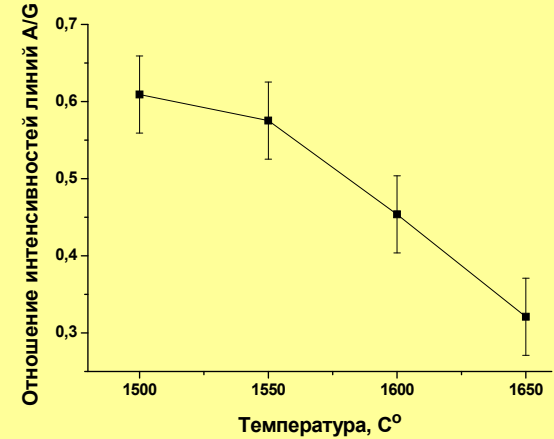
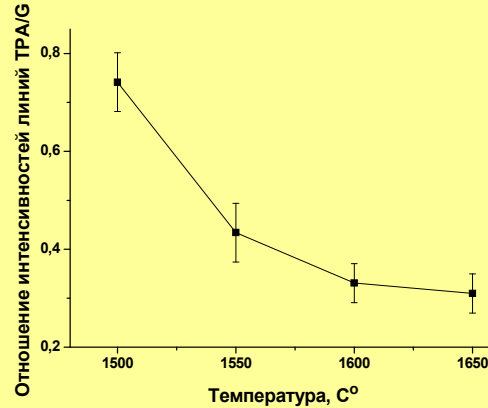
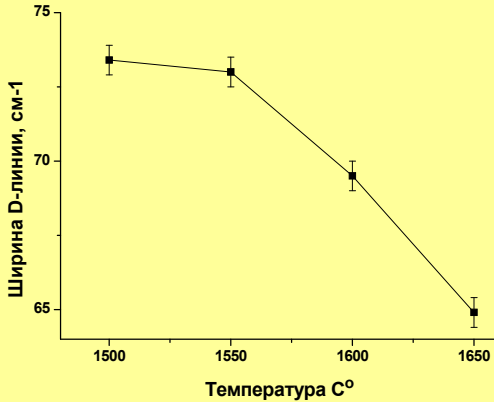


"Advanced Carbon Nanostructures" (ACN'2011)
 St.Petersburg, Russia, July 4-8, 2011



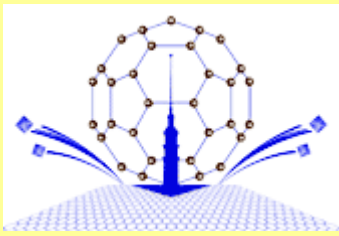
Presence of defects and amorphous phase.

Multishell nanographites (onion-like carbons, OLC) produced by annealing of detonation nanodiamonds



D-line width reflects the staking disorder.
TPA line intensity reflects the number of zig-zag chains.
A-line intensity reflects the quantity of amorphous carbon inside OLC.
D- and D'-line dispersion reflects electron and phonon dispersion curves.

Conclusion: Structural ordering with annealing.



"Advanced Carbon Nanostructures" (ACN'2011)
St.Petersburg, Russia, July 4-8, 2011



Conclusion.

Recent Raman studies demonstrated that the Raman spectroscopy presents a unique possibility for analysis of basic structural properties of the nanographites such as in- and out-of-plane crystallite size, out-of-plane stacking order, anisotropy of graphite ribbons, atomic structure at graphite edges and identification of single versus multi-graphene layers, as well as presence of defects and amorphization in nanographite samples.